Materials Research Letters

ISSN: 2166-3831 (Online) Journal homepage: www.tandfonline.com/journals/tmrl20

Magnetotransport in the MAX phases and their 2D derivatives: MXenes

Thierry Ouisse & Michel W. Barsoum

To cite this article: Thierry Ouisse & Michel W. Barsoum (2017) Magnetotransport in the MAX phases and their 2D derivatives: MXenes, Materials Research Letters, 5:6, 365-378, DOI: 10.1080/21663831.2017.1333537

To link to this article: https://doi.org/10.1080/21663831.2017.1333537

© 2017 The Author(s). Published by Informa UK Limited, trading as Taylor & Francis Group

Published online: 13 Jun 2017.

Submit your article to this journal

Article views: 4404

View related articles

View Crossmark data

Citing articles: 10 View citing articles

Full Terms & Conditions of access and use can be found at
https://www.tandfonline.com/action/journalInformation?journalCode=tmrl20

MATER. RES. LETT., 2017
VOL. 5, NO. 6, 365–378
https://doi.org/10.1080/21663831.2017.1333537

OPEN ACCESS Check for updates

Magnetotransport in the MAX phases and their 2D derivatives: MXenes

Thierry Ouisse[a] and Michel W. Barsoum [b]

[a]Université Grenoble-Alpes, CNRS, LMGP, Grenoble, France; [b]Department of Materials Science and Engineering, Drexel University, Philadelphia, PA, USA

ABSTRACT
Herein, we critically assess magnetotransport in the MAX phases and their 2D derivatives, MXenes. For some MAX phases, a simple, 2D hexagonal metal model describes weak-field magnetotransport of their nearly free electrons reasonably well. For others, experimental and/or theoretical Fermi surfaces need to be mapped—a crucial task required for true understanding. Even less is known about MXenes. The density of apparent mobile carriers in $Ti_3C_2T_x$—assuming a single-band model—is $\approx 1 \times 10^{14}$ cm^{-2} (10^{28} cm^{-3}), which justifies it being sometimes described as a 2D metal. Much work is needed before a clearer picture emerges.

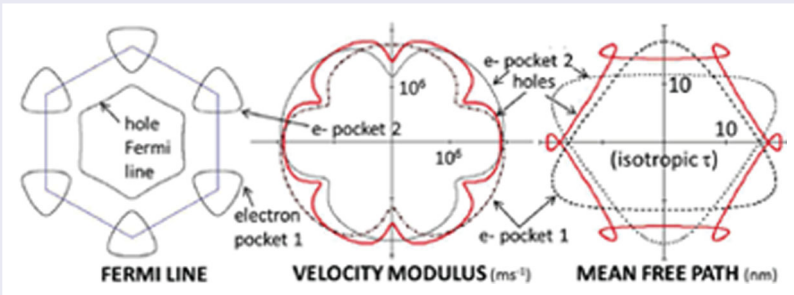

IMPACT STATEMENT
Magnetotransport in the MAX phases and their 2D derivatives MXene are critically reviewed for the first time. For some, a 2D hexagonal metal can explain magnetotransport; in others not.

ARTICLE HISTORY
Received 3 February 2017

KEYWORDS
MAX; MXenes; magnetotransport; Fermi lines; Fermi surfaces

1. Introduction

The $M_{n+1}AX_n$ or MAX phases are layered early transition metal ternary carbides and nitrides so called because they are composed of M, an early transition metal, A, a group A element (mostly 13 and 14) and X is C and/or N; n varies from 1 to 3. The MAX phase structure is composed of near close-packed planes of M atoms with the X atoms occupying all the octahedral sites between them. The latter are interleaved with layers of pure A. The cage around the A element is a right prism. Figure 1(a) shows the atomic arrangement of the $n = 1$ or 211 (top) and $n = 2$ or 312 (bottom) structures.

Most of the 211 phases—referred to then as H phases—Ti_3SiC_2 and Ti_3GeC_2 were discovered by Nowotny in Vienna in the sixties [2] and more or less lay dormant in the literature until a couple of papers published in 1996 and 1997 [3,4] showed that these solids to have an intriguing combination of metallic and ceramic properties. In 1999, the first prototype of an $n = 3$ or 413 phase was discovered [5], which led to the labeling these phases, MAX. Like metals, they are excellent conductors of electricity and heat and most readily machinable. Like ceramics, some are quite stiff and lightweight and some are exceptionally oxidation resistant. In 2011, it was discovered that by immersing Al-containing MAX phases in HF acid, it was possible to selectively etch the Al, resulting in two-dimensional, 2D, materials, that were labeled MXene to denote the removal of the A-group element and make the connection to another conducting 2D material, graphene [6,7].

This paper is concerned with electron transport in the MAX phases and their 2D derivatives, MXenes. The vast majority of MAX phases are metal-like conductors with a resistivity, ρ, that drops linearly with

CONTACT Michel W. Barsoum barsoumw@drexel.edu Department of Materials Science and Engineering, Drexel University, Philadelphia, PA 19104, USA

© 2017 The Author(s). Published by Informa UK Limited, trading as Taylor & Francis Group.
This is an Open Access article distributed under the terms of the Creative Commons Attribution License (http://creativecommons.org/licenses/by/4.0/), which permits unrestricted use, distribution, and reproduction in any medium, provided the original work is properly cited.

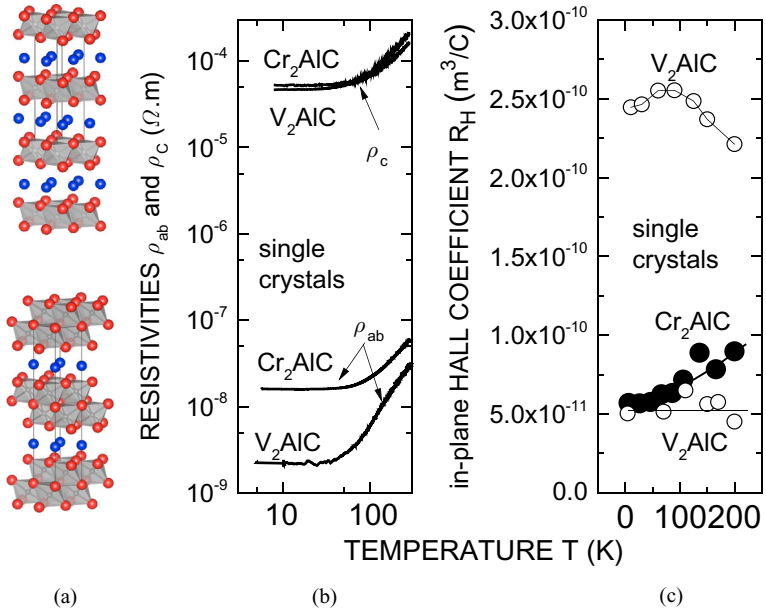

Figure 1. (a) 211 (top) and 312 (bottom) MAX stacking. Red are M atoms, blue are A atoms; C is in the center of the M-octahedra. Effect of temperature on magnetotransport in Cr_2AlC and V_2AlC single crystals. (b) log–log plot of resistivity along the basal planes and normal to them, vs. T and (c) in-plane Hall coefficient, R_H vs. T [1]. For reasons that are unclear, R_H for V_2AlC—measured on two different single crystals—yielded two sets of results (labeled V_2AlC) that were different.

decreasing temperatures, Ts. Not surprisingly, density functional theory, DFT, calculations show that their densities of states, DOS, at the Fermi level, $N(E_F)$, are quite substantial [8–10]. This prediction was experimentally confirmed for a large number of MAX phases [11–14]. Crucially, the DOS at E_F is dominated by the d–d orbitals of the M element [8,9]. At low Ts, ρ is dominated by defect scattering; at higher Ts, it is controlled by electron–phonon scattering [15].

In addition to the metal-like response, the vast majority of the MAX phases are characterized by small Hall coefficients, R_H, that sometimes change sign with increasing T, small magnetoresistances, MRs, and in some cases vanishingly small Seebeck coefficients over extended T ranges [16–19]. For example, in the case of Ti_3SiC_2, the Seebeck coefficient is almost vanishingly small over the 4K to 800 K temperature range [16,17]. It was thus clear early on that a conventional, one-band, model could not come close to explaining these results. An isotropic two-band model was thus assumed instead [17,18]. In the latter, there are four unknowns, the electron, n, and hole, p, concentrations, and their mobilities, μ_n and μ_p, respectively. Since there are only three equations relating these four values and since the Hall coefficient was small, the further assumption was made that either $n = p$ or $\mu_n = \mu_p$. With that assumption one could solve for all unknowns. For many MAX phases, n and p were found to be in the order to $1–3 \times 10^{27}\ m^{-3}$ [15]. The fact that, when estimated, the anisotropy ratio, ρ_c/ρ_{ab}, where ρ_c and ρ_{ab} are the resistivities along the c-axis and basal planes, respectively, was not too high rendered this idea plausible. For example, Scabarozi et al. [20] showed that when the resistivities of Ti_2GeC bulk samples and epitaxial thin films—of high quality, with residual resistance ratio, RRR, of 25 —were compared the maximum anisotropy ratio was estimated not to be > 2, contrary to DFT predictions [21].

Furthermore, Chaput et al. [22,23] carried out DFT calculations and made the case that the negligible thermopower observed in some MAX phases was because holes flowed along the basal planes and electrons flowed normal to them. Subsequent transport work supported this idea [24]. Based on the preponderance of evidence to date, most researchers have concluded that indeed holes are the majority carriers in the basal planes [1,22–25].

All was not well, however. At the end of 2013, one of us remarked: 'One of the most fundamental and unanswered questions concerning the transport properties of at least some of the MAX phases is why $n \approx p$ and $\mu_n \approx \mu_p$. There is no fundamental reason for that to be the case' [15]. Recently, Ouisse et al. [1] shed some light on this problem. Before delving into the details, they make a compelling case that while the two-band isotropic model may be useful in determining transport

parameters, these values have to be considered, at best, apparent values. Said otherwise, the electron concentration and mobility values obtained from such a model are more curve fitting parameters than actual physical values. Henceforth, in this paper, values extracted from a single or two-band isotropic model will be labeled as n_{app} and p_{app}.

The ultimate aim of this paper is to make the point while the magnetotransport in the MAX phases is complicated and depends crucially on the details of the Fermi surface, FS. We make the case, however, that in some cases, a simple 2D model can be quite useful indeed. This reassessment comes about because of two recent related developments: (i) the availability of relatively large MAX phase single crystals [26–28] and more importantly, (ii) the fact that the ρ_c/ρ_{ab} ratios for some of these single crystals are as high as 6000 (Figure 1(b)) [1]. These results are crucial and justify the simple 2D model described in the next section.

In-plane Hall coefficient, R_H, measurements were carried out on one Cr_2AlC and two V_2AlC single crystals. For reasons that are unclear the results for the latter were different (see Figure 1(c)). The R_H values around 5×10^{-11} m^3/C are typical of the MAX phases [15]. The values around 2.5×10^{-10} m^3/C, on the other hand, are higher.

2. MAX phases

2.1. Nearly free electron model, Fermi lines and 2D transport

Given the high ρ_c/ρ_{ab} ratios obtained, Ouisse et al. [1] applied a simple 2D, near free electron, NFE, model to a hexagonal metal, with the same lattice parameters as Ti_2AlC. The logic being that if one is to understand the 3D nature of conductivity in these materials, it behooves us to understand their 2D conductivity first. Figure 2(b) plots the projection, unto the basal plane, of Ti_2AlC, FS (Figure 2(a)), obtained from DFT calculations (all colors but red), along with the fit of the Fermi line given by the nearly free electron 2D model assuming $U = 0.35$ eV and $N = 6$, together with an appropriate interplane-induced splitting (red lines). Here, U is the Fourier component of the periodic potential for a wave vector joining the centers of two adjacent Brillouin zones and N is the total number of electrons per unit cell populating all partially filled bands. The excellent agreement between the simple 2D approach (red lines in Figure 2(b)) and the more involved DFT-based projections suggests that this approach has merit. Armed with this model, one can now plot the Fermi lines (Figure 2(c)), radial plot of the velocity (Figure 2(d)) and the mean free path (Figure 2(e)), assuming, $N = 6$, hole and electron

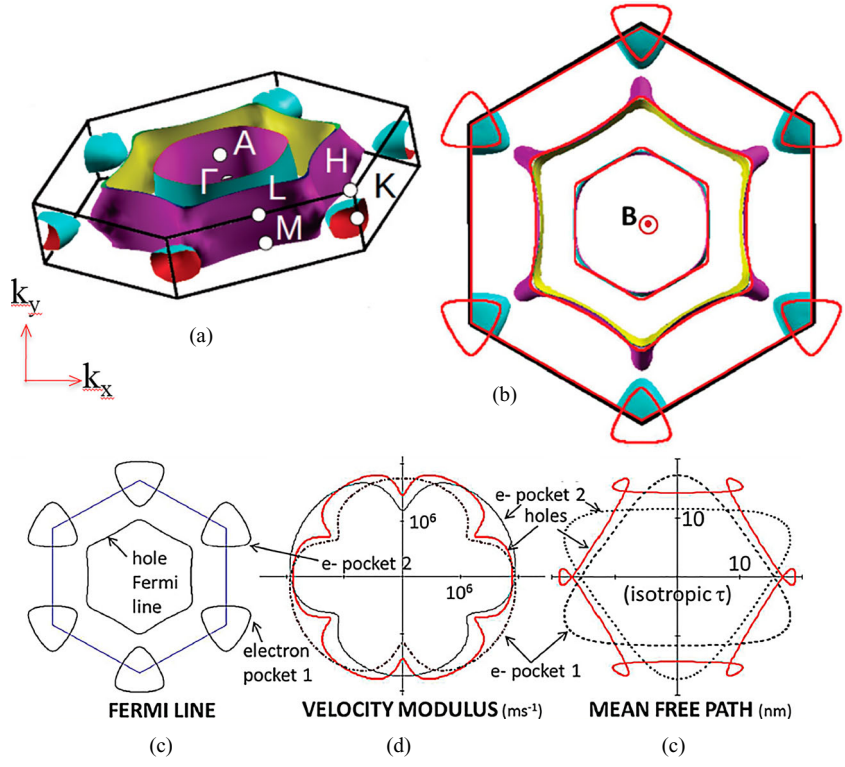

Figure 2. (a) DFT Fermi surface of Ti_2AlC, (b) projection of FS on basal plane (in color) and simple 2D Fermi lines assuming a simple NFE 2D model (in red). (c) 2D Fermi lines and corresponding, (d) velocity modulus and (e) mean free paths [1]. Applied magnetic field B is into the page.

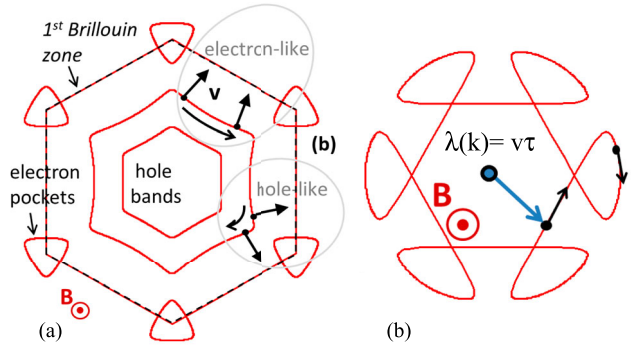

Figure 3. (a) Effect of Fermi line curvature on response of holes to B, applied along the c-axis of the hexagonal crystal. In some directions, the holes rotate clockwise and in others counterclockwise. (b) Mean free path, λ, of holes from (a). The net effect is determined by subtracting the areas of the outer loops from the area of the inner hexagon.

scattering times being respectively, $\tau_p = \tau_n = 10^{-14}$ s, $U = 0.75$ eV, $a = 0.304$ nm, $c = 1.36$ nm and four 2D M-planes per unit cell (bottom unit cell in Figure 1(a)). This simple model is able to explain a number of observations outlined in the introduction, as well as others that did not make much sense in an isotropic two-band model.

To understand the implications and ramifications of this 2D model, we start by noting that the hole FSs form open tubes, further justifying our 2D model, and allowing us to use the hole and electron Fermi lines given by that model (Figure 3(a)). The Boltzmann equation—at low B, and assuming a relaxation time approach is valid—for conventional metals is given by

$$\Delta f = -\left(1 + \frac{e\tau}{\hbar}(\mathbf{v} \times \mathbf{B})\frac{\partial}{\partial \mathbf{k}}\right)^{-1} e\tau \mathbf{v} \cdot \boldsymbol{\varepsilon} \frac{\partial f}{\partial E}, \quad (1)$$

where Δf is the out-of-equilibrium part of the carrier distribution function, f, $\boldsymbol{\varepsilon}$ is the electric field, $\mathbf{v}$ is the velocity, τ is the relaxation time and $\hbar$ is the reduced Plank's constant. Using Equation (1), the transport properties can be easily solved for by taking into account either the local curvature of the Fermi line or a variation of τ along it [1].

Analysis of basal plane transport is also made easier by using well-established theoretical results, and aid in understanding why the parameters extracted from a simple one- or two-carrier analysis bring about figures with no connection with the real electron and hole densities. In particular, the transverse 2D conductivity, in weak B field limit, is given by [29]

$$\sigma_{XY}^{2D} = \frac{2e^3}{h^2} A_l B, \quad (2)$$

where A_i is the oriented area spanned by the mean free path, $\boldsymbol{\lambda}$, when the wavevector, $\mathbf{k}$, cycles over one cyclotron orbit around the Fermi line. It shows that the transverse 2D conductivity only depends on $\boldsymbol{\lambda}$, which is the product of $\mathbf{v}$ and τ. Note that λ, $\mathbf{v}$ and τ may all possibly vary with $\mathbf{k}$. Furthermore, the combination of several bands leads to an overall ρ_{ab} and R_H of the form [29]:

$$R_H = \frac{\sum_i \sigma_{XY}^i}{\left(\sum_i \sigma_{XX}^i\right)^2 + \left(\sum_i \sigma_{XY}^i\right)^2} \frac{1}{B}, \quad (3)$$

$$\rho_{ab} = \frac{\sum_i \sigma_{XX}^i}{\left(\sum_i \sigma_{XX}^i\right)^2 + \left(\sum_i \sigma_{XY}^i\right)^2}. \quad (4)$$

Combining Equations (2) and (3), it is clear that a hole band and an electron band—with similar scattering processes—will tend to *cancel* the Hall coefficient, *independent of their carrier density ratios* (a case likely to apply if those bands are created from the splitting of a free Fermi line at the BZ boundaries in an NFE model). This simple consideration clearly shows that a vanishing R_H does *not* necessarily imply compensation by equal numbers of electrons and holes with similar mobilities.

Complexity does not end here, however, because even a single band can give rise to apparent compensated transport. Consider a hole band, as depicted in Figure 3(b), somewhat mimicking the hole Fermi line of Ti_2AlC (Figure 2(b)). Holes rotate along the Fermi line according to the semi-classical law of motion $\hbar\partial\mathbf{k}/\partial t = e\mathbf{v} \times \mathbf{B}$. At a given $\mathbf{k}$ value, $\mathbf{v}$ is perpendicular to the tangent of the Fermi line. If the curvature of the Fermi line changes sign, then the rotation of the velocity with time can switch from clockwise to anticlockwise, so that positively charged holes can rotate either clockwise or anticlockwise in *real* space (Figure 3(a)). This leads in turn to apparent compensation, manifest in the apparition of negatively oriented, outer flaps in the radial plot of λ, and to a corresponding decrease in R_H.

It also leads to the existence of an MR, even though one is dealing with a single band. Although not widely appreciated, such a phenomenon prevails in many metals [29,30] and is discussed in detail in [1] in the context of MAX phases. Owing to the predicted complexity of the latter, this makes the experimental determination of carrier densities from magnetotransport measurements problematic.

Starting with the 2D model shown in Figure 2(b) and assuming the existence of several bands the computations in [1] explain the following:

(a) Why $n_{app} \approx p_{app} \approx 10^{27}$ m^{-3}, despite the fact that the actual values of n and p can be quite different. A single-band model would give only holes

with $p_{\text{app}} \approx 4.6 \times 10^{28}\ \text{m}^{-3}$, while the actual values derived from the 2D model in this case are $p = 2 \times 10^{28}$ and $n = 2 \times 10^{27}\ \text{m}^{-3}$.

(b) Why an MR signature exists in the first place.

(c) Why R_{H} is typically small in many MAX phases. This is attributed to the fact that R_{H} is not only determined by n and p (p in this case), but also by the local curvature of the Fermi lines (Figure 3(a)). As the holes move along the basal planes in some directions, they are deflected by the magnetic field as electrons and in others as holes, namely clockwise and anticlockwise.

(d) Why R_{H} sometimes changes sign. In the 2D model presented above, it was assumed that $\tau_p = \tau_n = 10^{-14}$ s. However, if that ratio is changed slightly—say with T changes, a not unreasonable assumption given the anisotropies in atomic displacement parameter [31] (see below) —then R_{H} can actually change sign as has sometimes been observed [18].

(e) Why n_{app} and p_{app} are sometimes found to be a function of T [15]. As noted above, this observation cannot be easily reconciled with a conventional two-band model, for which metallic charge carrier densities are not expected to noticeably vary with T.

Based on these considerations, a fruitful approach to understanding transport in the MAX phases is to attempt to reproduce Figure 3 for a number of other MAX phases using as few parameters as possible. Once that is established, a 2D analysis—as carried out here for Ti_2AlC—should be carried out in order to match experiment and theory. This approach should work better for smaller, rather than larger, values of N. It should thus work reasonably well for Ti, Zr and, possibly, Hf-based MAX phases. Lastly, we note that this 2D model is also an excellent place to start to try and understand transport in MXenes (see below) that are by nature 2D.

2.2. Real Fermi surfaces

We now proceed from Fermi lines to Fermi surfaces, FSs. Figure 4 plots a number of MAX phases' FSs. The FSs are quite complicated and, at first glance, appear to be quite different. However, within the variability, there are some commonalities and differences:

(i) The FS shapes are determined more by the M elements than the A elements. This best seen by comparing the FSs of group 4 elements, Ti, Zr, Hf (Figure 4(a)–(c)) to those of group 5 elements, V and Nb (Figure 4(e,f)). The former are more similar to each other than they are to the latter. The FS of Mo_2GaC (group 6) is quite different from all others (Figure 4(g)).

(ii) The FSs of the Ti-containing 211 phases are quite comparable. This is best seen by comparing the FS of Ti_2AlC (Figure 2(a)) to that of Ti_2SnC (Figure 4(a)).

(iii) The FS of Ti_2AlC (Figure 2(a)), Ti_3AlC_2 (Figure 4(d)) and Ti_3SiC_2 (Figure 4(h)) share similarities. Note the difference between the latter two is in the value of N; it is one greater in Ti_3SiC_2. It is quite possible that Ti_2SnC, Ti_3AlC_2 and Ti_3SiC_2 can be modeled in the same way as Ti_2AlC [1].

None of these conclusions are too surprising since it has long been established that the DOS at E_{f} was dominated by the d–d orbitals of the M elements.

In particular, MAX phases are predicted to possess hole bands whose FS often adopts the shape of a bulged open tube along the c-axis, reminiscent of the spatial confinement into planes perpendicular to this direction [22,23,25,35]. Bulges and tube distortions can be very complicated, and the FSs of the various bands are often nested into one another (Figure 4). Electron bands are also found in most compounds, sometimes in the form of open tubes as for the holes, and sometimes exhibiting closed surfaces, thereby indicating delocalization along the c-axis [22,23,25]. Furthermore, not all MAX phases' FSs exhibit the same shape, even if there is a tendency to obtain Γ-centered nested hole tubes, with electron closed surfaces or open tubes centered at the K points. In other words, FSs that are not unlike those of our simple NFE approach. Interestingly, Cr_2AlC appears to be an exception in that Γ-centered nested electron tubes are surrounded by hole pockets centered at the M points [36].

Additional band splitting is due to topological differences between the various planes containing the transition metal atoms. However, not all phases are predicted to fit into this scheme [23,35], so that this should not be generalized. If we follow the predictions of the FS, then electrical transport should occur by both electrons and holes, with strong anisotropies lying either in the curvature of the FS or in the relaxation times, along with complications arising from the intricate contribution of a large number of occupied bands to the magnetotransport coefficients, or by anisotropies in the electron–phonon coupling. As discussed in the following sections, it is quite improbable that the electrical transport is dominated by any of these phenomena solely. Most probably, magnetotransport is determined by the overall contribution of various electrons and hole bands, by the anisotropies of the FSs and, in the phonon-limited regime, by anisotropies in electron–phonon coupling. Said otherwise, and as much as it would be desirable, it

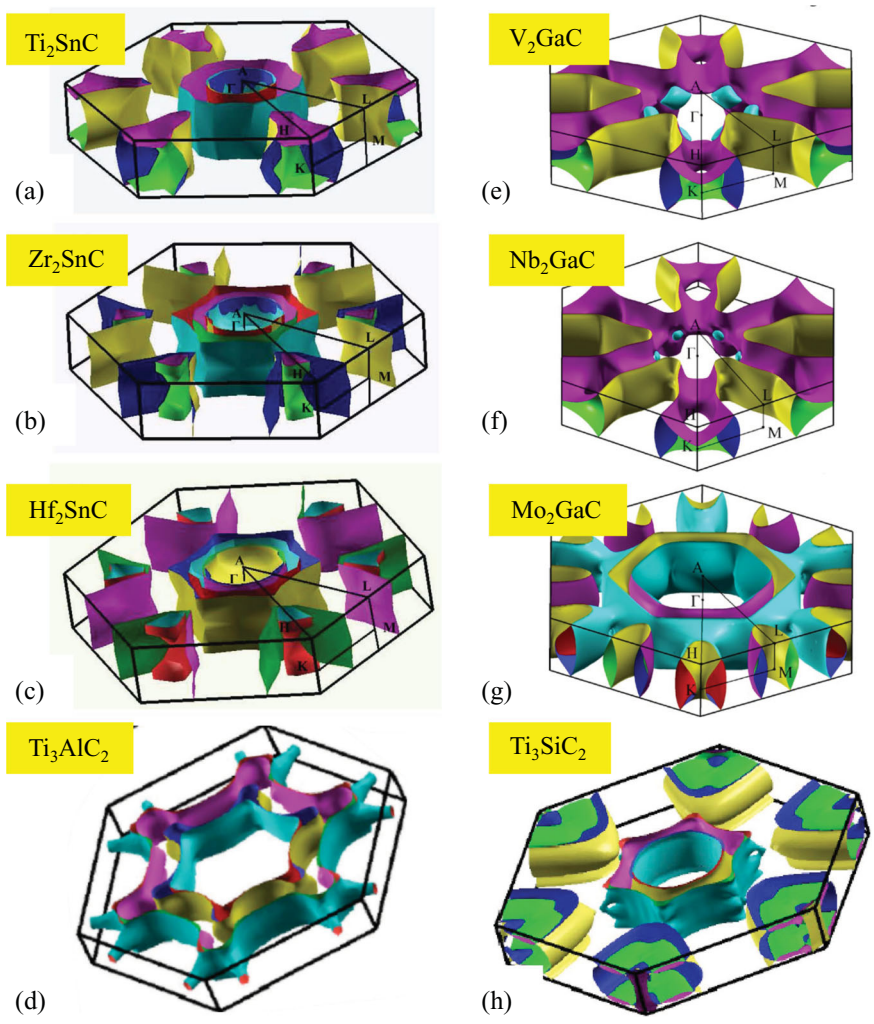

Figure 4. Fermi surfaces of, (a) Ti_2SnC [32], (b) Zr_2SnC [33], (c) Hf_2SnC [32], (d) Ti_3AlC_2 [23], (e) V_2GaC [34], (f) Nb_2GaC [34], (g) Mo_2GaC [34] and (h) Ti_3SiC_2 [23].

is unlikely that one transport model will explain transport in all MAX phases. The 2D model, however, should always be considered first before more sophisticated models are adopted.

2.3. Conduction in the c-direction and interplanar defects

Up to this point, the discussion was focused on transport in the basal planes. To shed light on the ρ_c/ρ_{ab} ratios, it is instructive to recap what is known about two other well-known layered solids: *oriented* pyrolytic graphite and high T_c cuprates. In hole-doped cuprates, measured ρ_c/ρ_{ab} ratios in the normal state can exceed 10^5 [37]; ratios for electron-doped cuprates vary from 10^3 to 10^4 [38]. In some graphite single crystals, ρ_c/ρ_{ab} exceeds 10^4 [39] and the intrinsic value is indeed still unknown. For pyrolytic graphite, ρ_c/ρ_{ab} varies from 10 to 3000, and depends almost exponentially on the deposition temperature [39]. This dependence is an important and crucial clue since it strongly suggests that *interlayer defects* are responsible for the out-of-plane conductivity (Figure 5(a)) and can result in MR. Indeed, this is the understanding to date. And since there is no reason to believe the situation is different herein we tentatively make the same conclusion. One needs to emphasize once again that the DOS of the A and X elements at E_F are quite small, sometimes vanishingly so.

It follows that the ρ_c/ρ_{ab} ratio can be used as an indirect measure of a single crystal/thin film's quality. In this, it is not unlike the idea that the RRR is also a measure of a sample's quality. We thus predict that as more perfect single crystals are produced, the ρ_c/ρ_{ab} ratio will increase accordingly. And while it is always dangerous to generalize based on a limited—two in this case—data set, the similarities in the nature of DOS at E_F for most MAX phases suggest that the intrinsic ρ_c/ρ_{ab} ratio for most of them will be quite high. These comments

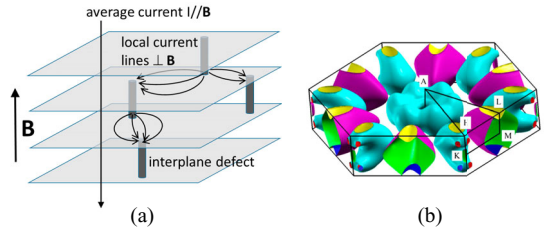

Figure 5. (a) Schematic showing how an imperfect 2D conducting material can nevertheless result in a current along the *c*-axis and give rise to an MR. (b) FS of Nb_2GeC [40].

notwithstanding, that does not necessarily mean it will be the case for all MAX phases. When the resistivity results obtained on a Ti_2GeC epitaxial thin film of high quality (with an RRR of $\approx$ 25) were compared to bulk properties of the same composition the anisotropy ratio—at $\approx$1.6—was found to be quite mild [20]. Interestingly, the FS of Nb_2GeC (Figure 5(b)) also suggests that this compound would act more like a 3D than a 2D conductor [40].

Quasi-2D systems usually exhibit unusual properties, mostly due to the correlations ruling the electron interactions that sometimes result in outstanding phenomena, ranging from high T_C superconductivity [38], to non-Fermi liquid properties [41]. Although all existing data indicate a strong electron–phonon coupling, the MAX phases are indeed not 'good' superconductors, with only a few phases exhibiting superconductivity at quite low T's [15]. However, some recently engineered MAX phases exhibit magnetic properties [42–45]. The impact of this magnetism on transport has just started to be assessed [46], and should bring interesting developments in the near future. More generally, correlations often result in departures from Fermi liquid theory [47,48], and to assess whether this is the case for the MAX phases remains to be explored. Although the MAX phases are neither outstanding superconductors nor intriguing topological insulators, this point is nevertheless worth being investigated.

2.4. Kohler's rule

Returning to the Boltzmann equation (Equation (1)) roughly speaking, since the term in brackets can be expanded as a function of $B\tau$, and no other term depends on B, this implies that any transport property should be a function of $B\tau$, and in turn on B/ρ. This is known as Kohler's rule (a more rigorous derivation where Kohler's rule is derived in tensor form can be found in [49]).

If Equation (1) is valid, then for a conventional Fermi liquid, plots of MR vs. B/ρ_0—or more usually $\Delta\rho/\rho_0$ vs. $(B/\rho_0)^2$ should be independent of T [49]. Said otherwise, if Kohler's rule is upheld, then the material can be considered a conventional Fermi liquid [49], as indeed observed for V_2AlC single crystals (Figure 6(a)) and preliminary results for Ti_3SiC_2 (not shown). In contradistinction, the same cannot be said about Cr_2AlC single crystals. With

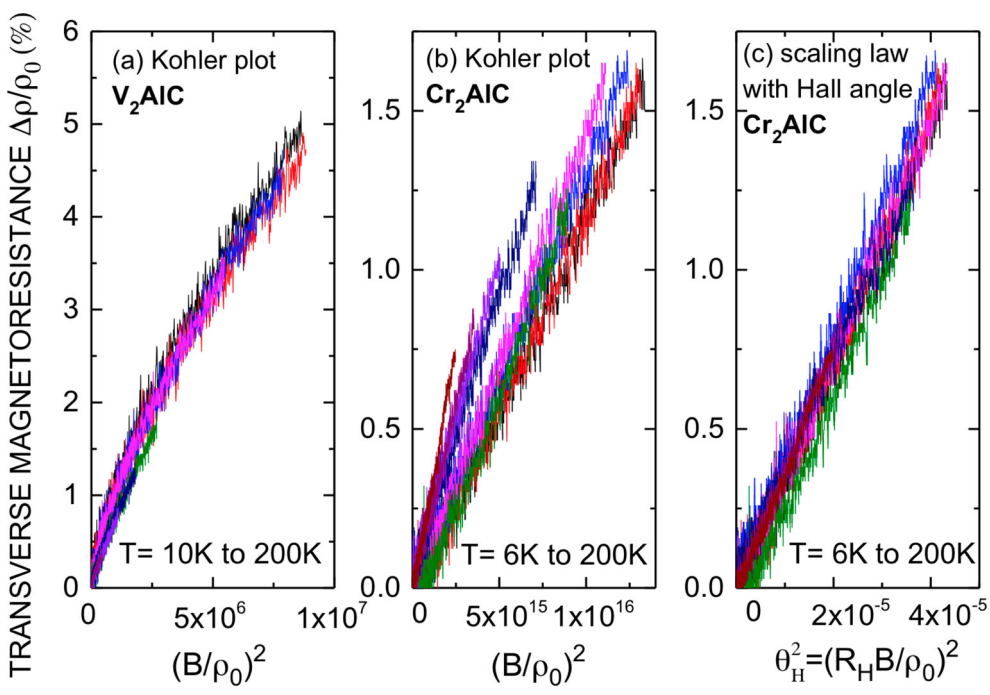

Figure 6. Effect of temperature on transverse magnetoresistance, MR, when plotted for single crystals of (a) V_2AlC; MR vs. $(B/\rho_0)^2$, (b) Cr_2AlC; MR vs. $(B/\rho_0)^2$ and (c) Cr_2AlC; MR vs. $(R_HB/\rho_0)^2$. Data taken from [1]. Each color line represents a different temperature.

data taken from Ref. [1], it is clear that Cr_2AlC not only does *not* obey Kohler's rule (Figure 6(b)). In this case, the scaling law is wherein MR is proportional to the Hall angle, namely $(\theta_H)^2$ viz. $(R_H B/\rho_0)^2$ is independent of T (Figure 6(c)). This response is thus similar to exotic, quasi-2D systems [50–52] such as high T_C superconducting cuprates [50], heavy Fermion compounds [51], or Fe superconducting pnictides in their normal state [52]. The explanations for the latter observation have been diverse: from non-Fermi liquid theories [48], local variations of the Hall angle on the Fermi line induced by antiferromagnetic interactions prevailing in localized parts of the Fermi line [47], to variations in carrier density with T, which is unlikely for quasi-2D metals with appreciable carrier densities, but yet advocated by some [53,54].

Identification of the physical mechanism leading to this scaling law should certainly be the subject of future research, for it might not only shed light on MAX phases, but also on other quasi-2D systems, where the controversy is still open, sometimes after decades of debate [49]. Cr_2AlC exhibits a higher thermal expansion coefficient than most other MAX phases [15], a larger electron–phonon coupling constant [15], and is predicted to be antiferromagnetic [55]. Whether any of those three properties plays a role has yet to be established.

The conventional two-band isotropic model with $n_{app} \cong p_{app}$ is the simplest one can imagine to explain the existence of a MR, leading to an MR: $\Delta\rho/\rho_0 = \mu_n\mu_p B^2$, and ρ_0 the resistivity for $B = 0$. Along with a simple one-band model, it is also currently the only tractable model for parameter extraction. However, it is worth recalling that any distortion in a spherical Fermi sphere must also give rise to an MR. As noted above, the complexity of the predicted FSs makes it highly doubtful the physical reality of the extracted carrier densities. The point is that not only several bands come into play, but that each band, considered alone, and as explained above, could give rise to an MR and vanishingly small R_H values.

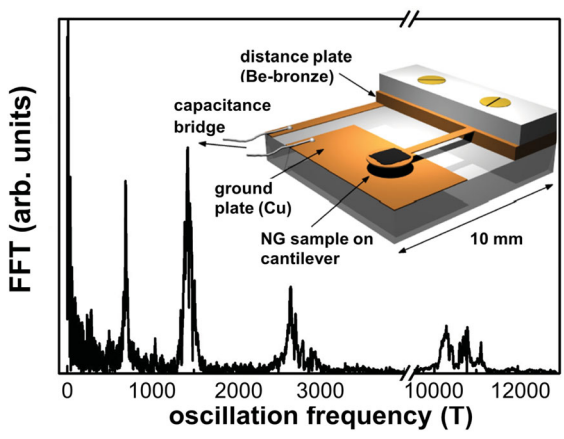

Figure 7. Frequency spectrum of the quantum de Haas van Alphen oscillations of the magnetization of a single crystal of Ti_3SiC_2 measured at $T = 1.3$ K. Here the applied magnetic field B is parallel to the c-axis (by courtesy of B. Piot, LNCMI, Grenoble).

Although no experimentally acquired FS landscape of any MAX phase can be found in the literature, preliminary data measured at LNCMI, Grenoble, definitely prove its complexity. As seen in Figure 7, measurements of de Haas van Alphen quantum oscillations of the magnetization with B in single-crystalline Ti_3SiC_2 clearly indicate the existence of multiple frequencies, and thus the contribution of many extremal orbits, a fact incompatible with the existence of two similar, isotropic electron and hole bands (the latter should give rise to a single frequency, independent of orientation of B). A better formulation of the carrier density problem would be: Why are the *apparent* electron and hole densities more or less equal in most MAX phases?

3. MXenes

Work on trying to understand transport in the MAX phases is roughly 20 years old and as shown herein more is still unknown than known. Their 2D counterparts—generated by etching the A layers from the MAX phases [6,7] —are only 5 years old and thus even much less is known about them. And while there is no doubt that magnetotransport in MXenes is more two dimensional than their parent phases, understanding it is probably even more challenging for several reasons, chief among them are: (i) when the A layers are etched, they are replaced by O, F and OH terminations (Figure 9(a)) [6,7,56]. (ii) In most cases, the interlayer space is populated by cations and water molecules [57], the exact arrangement of which is unknown. (iii) The exact stacking in multilayered particles can vary from particle to particle or from batch to batch. (iv) The possible presence of a large fraction of defects in the 2D sheets, especially when aggressive etchants such as 50% HF are used. In solids, in general and 2D solids in particular it is difficult to characterize and quantify point defects.

There have been few fundamental experimental transport studies on MXenes. The existing transport studies come in two flavors, those carried out on pressed MXene discs or thick films made by filtration. It is difficult to say anything about the fundamentals of transport from these studies since the control on flake-to-flake contact, arrangement, etc. is difficult to reproduce, let alone characterize. The most that can be extracted from such studies is the slope of ρ vs. T plots. For the most part, the slopes are positive, consistent with the metallic nature of MXenes. In some cases, the slopes are

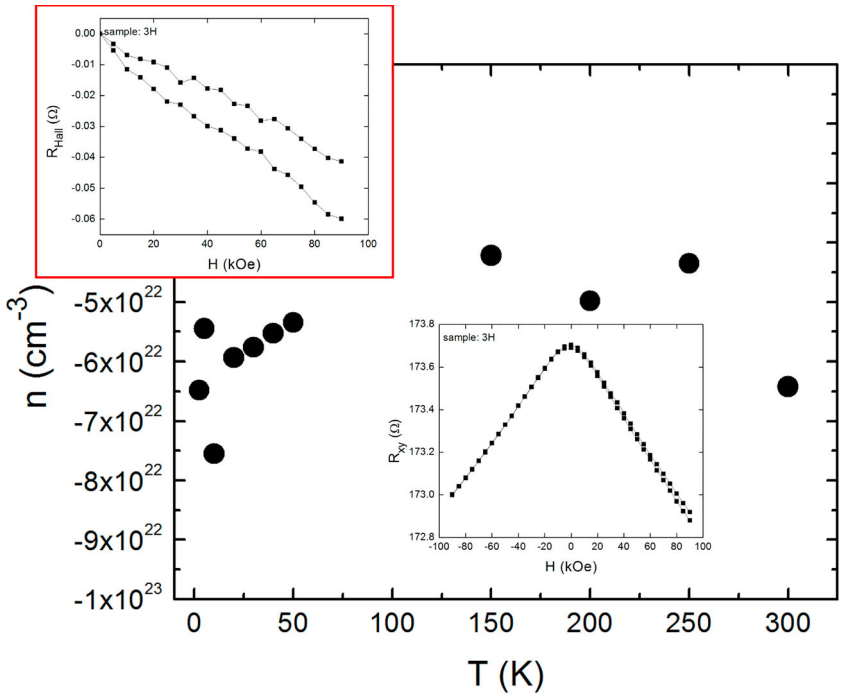

Figure 8. Charge carrier densities vs. T for etched, epitaxial $Ti_3C_2T_x$ thin films [61]. Top inset plots the Hall resistance, R_H, vs. applied magnetic field H up to 9 T. Lower inset plots ρ_{ab} vs. H up to 9 T. Note negative MR. (Results courtesy J. Halim, C. Smith and S. May, Drexel University, Philadelphia, PA).

negative, which prompted some to claim semiconductor-like characteristics [58–60]. However, since the negative slopes are most probably a result of a large number of defects, such a description may be misleading.

Plots of ρ vs. T can also be used to shed light on the transport mechanisms. For example, we showed that in the T range between 10 and 60 K, the T dependence of the conduction in $Ti_3C_2T_x$, in the form of etched epitaxial thin films [61], was compatible with a 2D variable range hopping mechanism. Interestingly, the MRs for these films were negative. In contrast, the MRs in Mo_2C [59] and $Mo_2TiC_2T_x$ [60] films were positive.

The other set of measurements, carried out mostly on $Ti_3C_2T_x$, in the form of epitaxial thin films [61], spin-coated films [62], single flakes [63,64] and individual multilayered particles, are more useful for shedding light on the transport problem because the arrangement of the flakes in these incarnations is more uniform. Figure 8 plots the carrier densities as a function of temperature for epitaxial thin films [61]. Top inset plots the Hall resistance, R_H, vs. applied magnetic field, lower inset plots ρ_{ab} vs. B both up to 9 T.

Results such as those shown in Figure 8 can—assuming a single-band model—be used to calculate the density of carriers and their mobilities. These values extracted from five such studies are summarized in Table 1. In one case, the conductivities of $Ti_3C_2T_x$ multilayers and $Ti_3C_2T_x$ particles were measured along, and normal to, the basal planes [67]. The reported anisotropy was about an order of magnitude between the in- and out-of-plane conductivities. However, at 24 and 1.4 S/cm, the conductivities were orders of magnitude lower compared to the rest

Table 1. Summary of room temperature conductivities, apparent carrier densities and mobilities, μ, for $Ti_3C_2T_x$.

$Ti_3C_2T_x$ morphology	Conductivity (S/cm)	n_{2D} (cm^{-2})	Carrier density (cm^{-3})	μ (cm^2/Vs)
Spin cast films [62]	4000 ± 400		$3 \pm 0.7 \times 10^{22}$	0.9 ± 0.1
Single flakes [63]	900	$8 \pm 3 \times 10^{14}$	$8 \pm 3 \times 10^{21}$ [a]	0.7 ± 0.2
Epitaxial films [61] [b]	1852		$5.6 \pm 0.3 \times 10^{22}$	0.2
Single flakes [64]	4580 ± 1000	$1 \pm 0.3 \times 10^{15}$ [c]	$1 \pm 0.3 \times 10^{22}$	2.6 ± 0.7
Tapes [65]	140	4×10^{13}		$\approx 10{,}000$

Note: For single flakes, the 2D carrier density, n_{2D}, is given assuming 1 nm thick flakes.
[a] In [63], the thickness of a single layer was assumed to be 0.75 nm. More recent work [66], measured the thickness to be closer to 1 nm, which is the value used here.
[b] See results in Figure 8.
[c] The results given in Table S2 in [64] implicitly assume a flake thickness of 1 nm, which is consistent with the most recent thickness value given in [66] and thus the more correct value. In the main part of the paper, the thickness is assumed to be 1.5 nm, which is incompatible with the results presented in Table S2 of Ref. [64]

of the values listed in Table 1. Similarly, the results of Lai et al. [65] —who report mobilities of 10,000 cm^2/Vs and carrier densities that are more than one order of magnitude lower than other reports (Table 1) —are clear outliers. These two studies are thus not included in what follows.

For reasons that are not quite clear, the carrier densities—again assuming a single-band model—measured, 3–5 $\times 10^{22}$ m^{-3}, on spincast [62] and epitaxial [61] films are higher than the single flake values (Table 1). In the first measurement ever on a single $Ti_3C_2T_x$ flake, the carrier density was reported to be $8 \pm 3 \times 10^{14}$ cm^{-2} [63]. A slightly higher value of $1 \pm 0.3 \times 10^{15}$ cm^{-2} was later reported by others [64]. Taken *in toto*, it is reasonable to conclude that the carrier density in $Ti_3C_2T_x$ is more or less fixed at $\approx 1 \times 10^{15}$ cm^{-2} or—assuming a thickness of 1 nm—1×10^{22} cm^{-3}. This is an important conclusion and suggests that this value is intrinsic to this MXene. Note, however, that this value is also an apparent value assuming a single-band model. The leitmotiv of this paper is that such values are at best effective values. To get the true values requires detailed knowledge of the FSs or lines in this case. Not surprisingly, the carrier mobilities, on the other hand, depend on flake quality and range between ≈ 0.2 and ≈ 3 cm^2/Vs [62–64].

Miranda et al. [63] were also the first to show that at room temperature it was not possible to modulate the drain-source currents using gate modulation, a not too surprising result given the metal-like density of carriers (Table 1) [63]. Here again, this was later confirmed by others [64]. Miranda et al. [63] did, however, see a change in mobilities at 2.5 K that they ascribed preliminarily to the complexities of the FS.

Interestingly, when the conductivities of $Ti_3C_2T_x$ single flakes and films made of the same flakes are compared, the difference is about an order of magnitude lower for the latter, implying that flake-to-flake electron transport—that has to go through the surface terminations—is surprisingly good [62,64]. From an application point of view, this is an important aspect that needs to be better understood. For example, one potential application for MXenes is as transparent conductive electrodes [62,68]. A good figure of merit, FOM, is the ratio of DC conductivity to an optical conductivity, or σ_{dc}/σ_{op} [69]. As shown in Table 2, films spin-coated from aqueous colloidal MXene solutions have the highest FOMs for this application. Note that the FOM of Ti_2CT_x [68] and $Ti_3C_2T_x$ [62] spin-coated films is comparable to those of chemically vapor deposited un-doped graphene [69]. Based on the current results, and when normalized per Ti atom, the spin-coated Ti_2CT_x films have to be considered the best [68].

Table 2. Summary of optoelectronic properties of MXene films.

Film	Conduct. (S cm^{-1})	σ_{dc}/σ_{op}	Absorbance coeffic. (cm^{-1})	Form	Refs
Ti_2CT_x	5,250	5	2.7×10^{-5}	Spincast	[68]
$Ti_3C_2T_x$	$6{,}500 \pm 800$	5	2.7×10^{-5}	Spincast	[62]
$Ti_3C_2T_x$	–	0.5		Spray coating	[70]
$Ti_3C_2T_x$	–	0.3		Spray coating	[70]
$Ti_3C_2T_x$	4,665			Filtered	[71]
$Ti_3C_2T_x$	3,092	3.1		Spincast	[72]

In contrast to the relative paucity of experimental papers, there have been a larger number of DFT papers, dealing with the electronic structure of MXenes, especially as a function of termination chemistries [6,67,73–77]. In the remainder of this section, we summarize the consensus from these calculations. They are:

(i) The MAX to MXene transformation in $Ti_3C_2T_x$ and Ti_2CT_x should result in an increase in the DOS at E_F.
(ii) Bare MXenes—with no terminations—should be metallic.
(iii) In the first report on $Ti_3C_2T_x$ [6], a small gap of 0.05 eV was predicted if it were OH-terminated and a 0.1 eV gap if it were F-terminated. And while these predictions have since been confirmed by others [78], as noted above, there is scant experimental evidence to back them up.
(iv) One may argue that such band gaps are small and could be missed experimentally. However, others have predicted large band gaps for O-terminated MXenes. For example, Khazaei et al. ([73,79]) predicted the following band gaps: 0.24 eV for Ti_2CO_2 and 0.88 eV for Zr_2CO_2 and 1 eV for Hf_2CO_2. Here, again these predictions await experimental verification.

Interestingly, the F, OH or O terminations introduce new bands—comprised mainly of p-orbitals—close to the M d bands. Two outcomes can be envisioned, as thoroughly described in a recent review paper by Khazaei et al. [79]. First, if hybridization of these new bands with the M d orbitals remains weak around E_F (e.g. with OH groups), then the main effect of the functionalization is to induce an electron transfer between the T's and the M's, and thus simply sweep the Fermi level through a d-band structure left roughly unmodified around E_F. In that case, a slight modification of the nature of the functionalization or of the stacking of the layers can result in substantial modification to the Fermi surface. A good example can be seen for the only published FS of an MXene, that of $Ti_3C_2T_x$ [67]. In this work, the authors examined a single flake (Figure 9(b)) and two stacking configurations: Bernal and simple hexagonal shown in

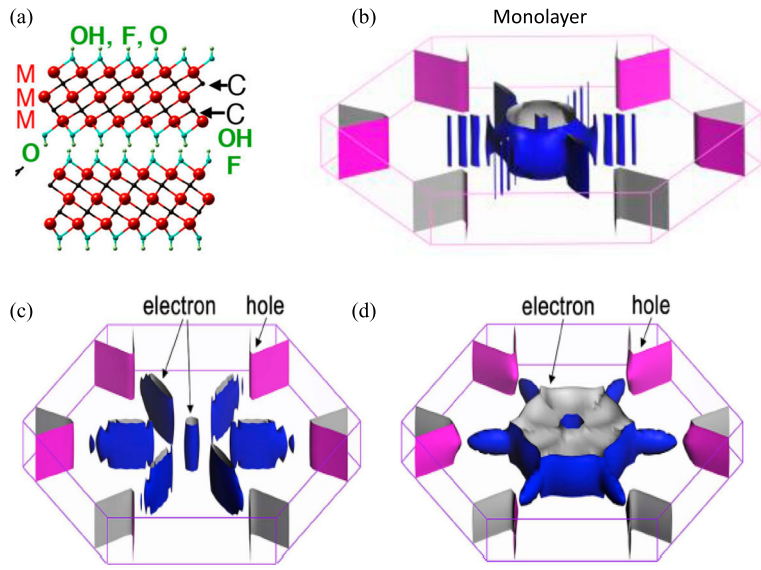

Figure 9. (a) Schematic of $M_{n+1}C_nT_x$ MXene showing OH, O and F terminations. (b) FS of a $Ti_3C_2(OH)_2$ monolayer. FS of multilayers assuming the MX-block stacking in (a) is, (c) Bernal or, (d) simple hexagonal [67].

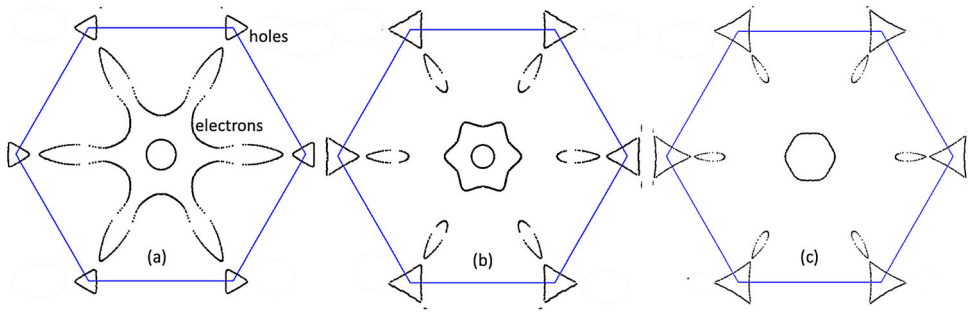

Figure 10. Fermi lines of termination-free 2D Ti_2C obtained from a simple tight-binding model using Harrison's parameters [80] and including only the M d and the C s and p orbitals. In going from left to right, E_F is shifted downwards by ≈ 20 meV each time. The similarities with the results shown in Figure 9(b,c) are striking.

Figure 9(c,d), respectively. Not surprisingly, dispersion along the *c*-axis was quite small confirming a 2D electronic structure. Interestingly, the FS is the reverse of the parent MAX phase (Figure 4(d)) in that the electrons are now in the center, with hole pockets around the edges.

Remarkably, sweeping E_F through an unmodified d-band can readily reproduce these results. To show this, in Figure 10, we plot the Fermi lines obtained by diagonalizing a simple and easy-to-solve tight-binding Hamiltonian involving only the M d and C p and s orbitals (M_2C phase, 14×14 Hamiltonian, parameters that are close to those given in [80]). Figure 10(a–c) is obtained by sweeping down E_F through rigid bands over intervals of the order of 20 meV. As rough as this model is, the similarity between these results and those obtained by DFT (Figure 9) is striking.

As noted in Khazaei et al. [79], the second main effect occurs when the hybridization between the p T and C p or M d orbitals becomes more substantial. Then, not only is the band structure appreciably modified, even in the vicinity of the original Fermi-level position in the pristine MXene, but the Fermi-level shift is predicted to become large enough so as to drive E_F in the forbidden gap separating the d bands from the hybridized p T and C p bands. If these predictions are verified, then they would in turn render MXenes direct competitors to the semiconducting members of the transition metal di-chalcogenide family.

An interesting magnetotransport feature that has been observed for various MXenes has been a negative MR [61]. In addition, observation of a dependence of the conductivity with temperature T proportional to $\exp(-(T_0/T)^{1/3})$ in the low T regime strongly suggests

that variable range hopping is operative [59,61]. Such a mechanism in turn suggests that we are dealing with, (i) a heavily doped semiconductor, (ii) a highly disordered metallic phase exhibiting a mobility edge or (iii) granular metals where the energy barriers are formed in between the metal grains. At this time, the published results do not allow us to discriminate between those possibilities. Higher T measurements could indicate the presence of an activated regime in the resistivity with an activation energy corresponding to the depth of the impurity band in the band gap, or to the mobility edge of a highly disordered metal. Gated devices fabricated with these phases should also allow one to definitely demonstrate or refute their semiconducting nature.

4. Perspectives and final thoughts

As single-crystalline/single flake transport data have only started to be measured there is still much to be done before a thorough picture of the physical mechanisms governing magnetotransport in the MAX phases and MXenes, including the anisotropies, emerges. The high number of existing phases makes the task a hard one, especially given the fact that many phases cannot be easily produced in single crystal form with techniques such as solution growth, due to the poor carbon solubility in liquids containing, e.g. Ga, In or Sn, or in a suitable crystal orientation and with a high enough quality in the case of thin deposited or converted single-crystalline layers. Ironically enough, since it is somewhat easier to deposit MXene single flakes, and measure their transport properties [63,64,81], we may learn more about transport in the MAX phases from their much younger 2D cousins.

To conclude for a better understanding of magnetotransport in the MAX phases, the following experiments—to be carried out on single crystals—are recommended:

(i) Experimentally assess the Fermi surface shapes and how well they conform to those obtained from *ab initio* calculations. This can be obtained either by deciphering dHvA oscillations in single crystals (in progress at LNCMI, Grenoble, see Figure 7) or by a direct measurement using Angle Resolved PhotoEmission Spectroscopy or ARPES (in progress at Nagoya University).
(ii) Measurement of thermopower as a function of orientation.
(iii) Thorough investigation of magnetotransport properties in magnetic MAX phases.
(iv) Assess correlation between anisotropy ratio and crystal quality.
(v) Determine the influence of defects such as vacancies and bulk ripplocations [82] on electronic properties.
(vi) Understand why Cr_2AlC—and possibly others—exhibits the same scaling law as 'exotic' quasi-2D compounds, whereas others, such as V_2AlC and Ti_3SiC_2, do not.
(vii) Find a method to isolate electron—phonon coupling anisotropy and measure it.
(viii) Find a general explanation for the $n_{\mathrm{app}} = p_{\mathrm{app}}$ rule, in a way more elegant than relying on numerical integrations of the transport properties along the calculated Fermi lines.
(ix) Determine whether all bulk MAX single crystals exhibit high anisotropy resistivity ratios.
(x) Determine whether magnetotransport is affected by magnetic breakdown phenomena, since many bands are predicted to get quite close to each another by *ab initio* DFT calculations.
(xi) Try to discover the elusive MXenes with band gaps and/or magnetic properties.

Acknowledgements

Many thanks are due to B. Piot (LNCMI) for allowing us to use some yet unpublished data (Figure 7), and to L. Shi (LMGP and UCL) and B. Hackens (UCL) for their help in treating the magnetotransport data already published in [1].

Disclosure statement

No potential conflict of interest was reported by the authors.

Funding

T. Ouisse was supported by Agence Nationale de la Recherche [project ANR-13-BS09-0024]. M.W.B. acknowledges the support of the Chair of excellence from the UGA Nanosciences Foundation, Grenoble, France

ORCID

Michel Barsoum http://orcid.org/0000-0001-7800-3517

References

[1] Ouisse T, Shi L, Piot BA, et al. Magnetotransport properties of nearly-free electrons in two-dimensional hexagonal metals and application to the $M_{n+1}AX_n$ phases. Phys Rev B. 2015;92:045133.
[2] Nowotny H. Strukturchemie Einiger Verbindungen der Ubergangsmetalle mit den elementen C, Si, Ge, Sn. Prog Solid State Chem. 1970;2:27–30.
[3] Barsoum MW, El-Raghy T. Synthesis and characterization of a remarkable ceramic: Ti_3SiC_2. J Amer Cer Soc. 1996;79:1953–1956.
[4] Barsoum MW, Brodkin D, El-Raghy T. Layered machinable ceramics for high temperature applications. Scrip Met Mater. 1997;36:535–541.

[5] Barsoum MW, Farber L, Levin I, et al. High-resolution transmission electron microscopy of Ti_4AlN_3, or $Ti_3Al_2N_2$ revisited. J Amer Cer Soc. 1999;82:2545–2547.
[6] Naguib M, Kurtoglu M, Presser V, et al. Two dimensional nanocrystals produced by exfoliation of Ti_3AlC_2. Adv Mater. 2011;23:4248–4253.
[7] Naguib M, Mashtalir O, Carle J, et al. Two-dimensional transition metal carbides. ACS Nano. 2012;6:1322–1331.
[8] Medvedeva N, Novikov D, Ivanovsky A, et al. Electronic properties of Ti_3SiC_2-based solid solutions. Phys Rev B. 1998;58:16042–16050.
[9] Hug G, Fries E. Full-potential electronic structure of Ti_2AlC & Ti_2AlN. Phys Rev B. 2002;65:113104.
[10] Ahuja R, Eriksson O, Wils JM, et al. Electronic structure of Ti_3SiC_2. Appl Phys Lett. 2000;76:2226–2228.
[11] Lofland SE, Hettinger JD, Meehan T, et al. Electron-phonon coupling in MAX phase carbides. Phys Rev B. 2006;74:174501.
[12] Drulis MK, Czopnik A, Drulis H, et al. Low temperature heat capacity and magnetic susceptibility of Ti_3SiC_2. J Appl Phys. 2004;95:128–133.
[13] Drulis MK, Czopnik A, Drulis H, et al. On the heat capacities of Ti_3GeC_2. Mater Sci Eng B. 2005;119:159–163.
[14] Drulis MK, Drulis H, Gupta S, et al. On the heat capacities of M_2AlC (M = Ti, V, Cr) ternary carbides. J Appl Phys. 2006;99:093502.
[15] Barsoum MW. MAX phases: properties of machinable carbides and nitrides. Weinheim: Wiley VCH GmbH; 2013.
[16] Yoo HI, Barsoum MW, El-Raghy T. Ti_3SiC_2: a material with negligible thermopower over an extended temperature range. Nature. 2000;407:581–582.
[17] Finkel P, Hettinger JD, Lofland SE, et al. Magnetotransport properties of the ternary carbide Ti_3SiC_2: hall effect, magnetoresistance and magnetic susceptibility. Phys Rev B. 2001;65:035113.
[18] Finkel P, Barsoum MW, Hettinger JD, et al. Low-temperature transport properties of nanolaminates Ti_3AlC_2 and Ti_4AlN_3. Phys Rev B. 2003;67:235108.
[19] Hettinger JD, Lofland SE, Finkel P, et al. Electrical transpot, thermal transport and elastic properties of M_2AlC (M = Ti, Cr, Nb and V) phases. Phys Rev B. 2005;72:115120.
[20] Scabarozi TH, Eklund P, Emmerlich J, et al. Weak electronic anisotropy in the layered nanolaminate Ti_2GeC. Solid State Commun. 2008;146:498–501.
[21] Zhou YC, Dong HY, Wang XH, et al. Electronic structure of the layered ternary carbides Ti_2SnC and Ti_2GeC. J Phys: Condens Matter. 2000;12:9617–9627.
[22] Chaput L, Hug G, Pecheur P, et al. Ansiotropy and thermopower is Ti_3SiC_2. Phys Rev B. 2005;71:121104(R).
[23] Chaput L, Hug G, Pecheur P, et al. Thermopower of the 312 MAX phases Ti_3SiC_2, Ti_3GeC_2, and Ti_3AlC_2. Phys Rev B. 2007;75:035107.
[24] Magnuson M, Mattesini M, Van Nong N, et al. The electronic-structure origin of the anisotropic thermopower of nanolaminated Ti_3SiC_2 determined by polarized X-ray spectroscopy. Phys Rev B. 2012;85:195134.
[25] Mauchamp V, Yu W, Gence L, et al. Anisotropy of the resistivity and charge-carrier sign in nanolaminated Ti_2AlC: experiment and ab initio calculations. Phys Rev B. 2013;87:235105.
[26] Ouisse T, Sarigiannidou E, Chaix-Pluchery O, et al. High temperature solution growth and characterization of Cr_2AlC single crystals. J Crystal Growth. 2013;384:88–95.
[27] Shi L, Ouisse T, Sarigiannidou E, et al. Synthesis of single crystals of V_2AlC phase by high-temperature solution growth and slow cooling technique. Acta Mater. 2015;83:304–309.
[28] Mercier F, Chaix-Pluchery O, Ouisse T, et al. Raman scattering from Ti_3SiC_2 single crystals. Appl Phys Letters. 2011;98:081912.
[29] Ong NP. Geometric interpretation of the weak-field Hall conductivity in two-dimensional metals with arbitrary Fermi surface. Phys Rev B. 1991;43:193–201.
[30] Banik NC, Overhauser AW. Hall coefficient of a holelike Fermi surface. Phys Rev B. 1978;18:1521–1532.
[31] Lane NJ, Vogel S, Caspi E, et al. High-temperature neutron diffraction study of Ti_2AlC, Ti_3AlC_2 and $Ti_5Al_2C_3$. J Appl Phys. 2013;113:183519.
[32] Kanoun MB, Goumri-Said S, Reshak AH. Theoretical study of mechanical, electronic, chemical bonding and optical properties of Ti_2SnC, Zr_2SnC, Hf_2SnC and Nb_2SnC. Comp Mater Sci. 2009;47:491–500.
[33] Kanoun MB, Goumri-Said S, Reshak AH, et al. Electro-structural correlations, elastic and optical properties among the nanolaminated ternary carbides Zr_2AC. Solid State Sci. 2010;12:887.
[34] Shein IR, Ivanovskii AL. Structural, elastic, electronic properties and Fermi surface for superconducting Mo_2GaC in comparison with V_2GaC and Nb_2GaC from first principles. Physica C. 2010;470:533–537.
[35] Mattesini M, Magnuson M. Electronic correlation effects in the Cr_2GeC $M_{n+1}AX_n$ phase. J Phys Cond Matter. 2013;25:035601.
[36] Jia G-Z, Yang L-J. Ab initio calculations for properties of Ti_2AlN and Cr_2AlC. Physica B. 2010;405:4561–4564.
[37] Martin S, Fiory AT, Fleming RM, et al. Temperature-dependence of the resistivity tensor in superconducting $BI_2Sr_{2.2}Ca_{0.8}Cu_2O_8$ crystals. Phys Rev Lett. 1988;60:2194.
[38] Armitage NP, Fournier P, Greene RL. Progress and perspectives on electron-doped cuprates. Rev Mod Phys. 2010;82:2421.
[39] Klein CA. Electrical properties of pyrolytic graphites. Rev Mod Phys. 1962;34:56.
[40] Shein IR, Ivanovskii AL. Structural, elastic, and electronic properties of new 211 MAX phase Nb_2GeC from first-principles calculations. Physica B. 2013;410:42–48.
[41] Shishido H, Shibauchi T, Yasu K, et al. Tuning the dimensionality of the heavy fermion compound $CeIn_3$. Science. 2010;327:980.
[42] Ingason AS, Dahlqvist M, Rosen J. Magnetic MAX phases from theory and experiments; a review. J Phys Cond Matter. 2016;28:433003.
[43] Dahlqvist M, Ingason AS, Alling B, et al. Magnetically driven anisotropic structural changes in the atomic laminate Mn_2GaC. Phys Rev B. 2016;93:014410.
[44] Liu Z, Waki T, Tabata Y, et al. Mn-doping-induced itinerant-electron ferromagnetism in Cr_2GeC. Phys Rev B. 2014;89:054435.
[45] Tao QZ, Hu CF, Lin S, et al. Coexistence of ferromagnetic and a re-entrant cluster glass state in the layered quaternary $(Cr_{1-x},Mn_x)_2GeC$. Mater Res Lett. 2014;2:192–198.

[46] Lin S, Tong P, Wang BS, et al. Magnetic and electrical/thermal transport properties of Mn-doped $Mn_{n+1}AX_n$ phase compounds $Cr_{2-x}Mn_xGaC$ ($0 < \times < 1$). J Appl Phys. 2013;113:053502.
[47] Anderson PW. Hall-effect in the 2-dimensional luttinger liquid. Phys Rev Lett. 1991;67:2092.
[48] Kontani H. Anomalous transport phenomena in Fermi liquids with strong magnetic fluctuations. Rep Prog Phys. 2008;71:026501.
[49] Luo N, Miley GH. Kohler's rule and relaxation rates in high-T-c superconductors. Physica C. 2002;371:259.
[50] Harris M, Yan FY, Matl P, et al. Violation of Kohler's rule in the normal state magnetoresistance of $YBau_3O_{7-\delta}$ and $La_2Sr_xCuO_4$. Phys Rev Lett. 1995;75:1391.
[51] Nakajima Y, Shishido H, Nakai H, et al. Non-Fermi liquid behavior in the magnetotransport of $CeMln_5$ (M: Co and Rh): striking similarity between quasi two-dimensional heavy fermion and high-T-c cuprates. J Phys Soc Japan. 2007;76:024703.
[52] Kasahara S, Shibauchi T, Hashimoto K, et al. Evolution from non-Fermi- to Fermi-liquid transport via isovalent doping in $BaFe_2(As_{1-x}P_x)_2$ superconductors. Phys Rev B. 2010;81:184519.
[53] Ghosh N, Bharathi A, Satya AT, et al. Kohler's rule in $Ba_{1-x}K_xFe_2As_2$. Solid State Commun. 2010;150:1940.
[54] Barišić N, Chan MK, Veit MJ, et al. Hidden Fermi-liquid behavior throughout the phase diagram of the cuprates. arXiv:150707885.
[55] Dahlqvist M, Alling B, Rosen J. Correlation between magnetic state and bulk modulus of Cr_2AlC. J Appl Phys. 2013;113:216103.
[56] Halim J, Cook KM, Naguib M, et al. X-ray photoelectron spectroscopy of Two-dimensional transition metal carbides (MXenes). Appl Surf Sci. 2016;362:406–417.
[57] Ghidiu M, Halim J, Kota S, et al. Ion exchange and solvation reactions in 2D Ti_3C_2 MXene. Chem Mater. 2016;28:3507–3514.
[58] Anasori B, Xie Y, Beidaghi M, et al. Two-dimensional, ordered, double transition metal carbides (MXenes). ACS Nano. 2015;9:9507–9516.
[59] Halim J, Kota S, Lukatskaya M, et al. Synthesis and characterization of 2D molybdenum carbide (MXene). Adv Funct Mater. 2016;26:3118–3127.
[60] Anasori B, Shi C, Moon EJ, et al. Control of electronic properties of 2D carbides (MXenes) by manipulating their transition metal layers. Nanoscale Horizon. 2016;1:227–234.
[61] Halim J, Lukatskaya M, Cook KM, et al. Transparent conductive two-dimensional titanium carbide thin filims. Chem Mater. 2014;26:2374–2381.
[62] Dillon AD, Ghidiu M, Krick A, et al. Highly-conductive, optical-quality films from solution-processed 2D titanium carbide (MXene). Adv Funct Mater. 2016;26:4162–4168.
[63] Miranda A, Halim J, Barsoum MW, et al. Electronic properties of freestanding $Ti_3C_2T_x$ MXene monolayers. App Phys Lett. 2016;108:033102.
[64] Lipatov A, Alhabeb M, Lukatskaya MR, et al. Effect of synthesis on quality, electronic properties and environmental stability of individual monolayer Ti_3C_2 MXene flakes. Adv Electron Mater. 2016;2:1600255.
[65] Lai S, Jeon J, Jang SK, et al. Surface group modification and carrier transport property of layered transition metal carbides (Ti_2CT_x, T: -OH, -F and –O). Nanoscale. 2015;7:19390–19396.
[66] Miranda A, Halim J, Lorke A, et al. Rendering $Ti_3C_2T_x$ (MXene) monolayers visible. Mater Res Lett. 2017; http://dx.doi.org/10.1080/21663831.2017.1280707.
[67] Hu T, Zhang H, Wang J, et al. Anisotropic electronic conduction in stacked two-dimensional titanium carbide. Sci Rep. 2015;5:16329.
[68] Ying G, Dillon AD, Fafarman AT, et al. Transparent, conductive solution processed spincast 2D Ti_2CT_x (MXene) films. Mater Res Lett. 2017; doi:10.1080/21663831.2017.1296043
[69] De S, Coleman JN. Are there fundamental limitations on the sheet resistance and transmittance of thin graphene films? ACS Nano. 2010;4:2713–2720.
[70] Hantanasirisakul K, Zhao MQ, Urbankowski P, et al. Fabrication of $Ti_3C_2T_x$ MXene transparent thin films with tunable optoelectronic properties. Adv Electron Mater. 2016;2:1600050.
[71] Shahzad F, Alhabeb M, Hatter CB, et al. Electromagnetic interference shielding with 2D transition metal carbides (MXenes). Science. 2016;353:1137–1140.
[72] Mariano M, Mashtalir O, Antonio FQ, et al. Solution-processed titanium carbide MXene films examined as highly transparent conductors. Nanoscale. 2016;8:16371–16378.
[73] Khazaei M, Arai M, Sasaki T, et al. Novel electronic and magnetic properties of two-dimensional transition metal carbides and nitrides. Adv Funct Mat. 2013;23:2185–2192.
[74] Xie Y, Kent PRC. Hybrid density functional study of structural and electronic properties of functionalized $Ti_{n+1}X_n$ ($X = C, N$) monolayers. Phys Rev B. 2013;87:235441.
[75] Enyashin AN, Ivanovskii AL. Atomic structure, comparative stability and electronic properties of hydroxylated Ti_2C and Ti_3C_2 nanotubes. Comp Theor Chem. 2012;989:27–32.
[76] Enyashin AN, Ivanovskii AL. 2D titanium carbonitrides and their hydroxylated derivatives: structural, electronic properties and stability of MXenes $Ti3C_{2-x}N_x$ and $Ti_3C_{2-x}N_x(OH)_2$. J Solid State Chem. 2013;207:42–48.
[77] Zha XH, Luo K, Li QW, et al. Role of the surface effect on the structural, electronic and mechanical properties of the carbide MXenes. Europhys Lett. 2015;111:6.
[78] Tang Q, Zhou Z, Shen P. Are MXenes promising anode materials for Li Ion batteries? Computational studies on electronic properties and Li storage capability of Ti_3C_2 and $Ti_3C_2X_2$ ($X = F, OH$) monolayer. J Amer Chem Soc. 2012;134:16909–16916.
[79] Khazaei M, Ranjbar A, Arai M, et al. Electronic properties and applications of MXenes: a theoretical review. J Mater Chem C. 2017;5:2488.
[80] Harrison W. Elementary electronic structure. Singapore: World Scientific; Singapore 2011.
[81] Sang X, Xie Y, Lin M-W, et al. Atomic defects in monolayer titanium carbide ($Ti_3C_2T_x$) MXene. ACS Nano; 2016;10:9193–200.
[82] Gruber J, Lang A, Griggs J, et al. Evidence for bulk ripplocations in layered solids. Sci Rep. 2016;6:33451.